J. Fluid Mech. (2011), *vol.* 669, *pp.* 32–54. © Cambridge University Press 2011
doi:10.1017/S0022112010004891

Optimal two-layer approximation for continuous density stratification

R. CAMASSA AND R. TIRON†

Department of Mathematics, University of North Carolina, Chapel Hill, NC 27599-3250, USA

(Received 3 March 2010; revised 9 September 2010; accepted 16 September 2010;
first published online 5 January 2011)

Two-layer fluids of finite depth under gravity are the simplest configuration capable of supporting internal wave motion. The extent to which such systems can be used to provide quantitative information on smoothly stratified fluids, in configurations relevant for geophysical applications, is analysed and a model of practical interest derived. The model is based on long-wave asymptotic expansions and on first-principle criteria for an optimal choice of effective two-layer parameters for the incompressible, smoothly stratified Euler equations. The accuracy of the model is extensively tested, via fully resolved numerical computations, on the class of travelling wave solutions supported by smooth stratification systems. It is found that, despite the severe restrictions posed by the discrete two-layer density assumption, solitary wave solutions corresponding to experimentally realizable parametric values can be accurately predicted, in both wave and fluid parcel markers, such as phase speed and density fields, respectively. Thanks to this analysis, explicit closed-form solutions are available for all relevant physical quantities. The agreement between the simple, optimized two-layer model and the parent smooth-stratification Euler system persists up to extreme cases, such as that of internal fronts, and even up to thicknesses of the pycnocline comparable to that of the effective layers.

Key words: internal waves, shallow water flows, stratified flows

1. Introduction

Density stratifications encountered in geophysical applications can often be viewed as two layers of approximately constant density fluids separated by an intermediate, diffused layer (the pycnocline) in which the density varies smoothly between the two limiting values. When the pycnocline is thin, a two-layer system successfully describes wave motion supported by such configurations, as comparisons between theory and experiments (e.g. in Grue *et al.* 1999) reveal. Typically, the interface position of the two-layer system is chosen at the inflection point of the density profile, while the densities of the two layers are set by the extrema of the density profile. Mathematically, the convergence of smoothly stratified Euler system solutions to those of the two-layer system in the limit of zero pycnocline thickness has been established rigorously (see e.g. James 2001) for square-integrable density norms.

The two-layer system is by far the simplest configuration supporting internal wave motion, and consequently both asymptotic and full Euler models for wave motion in

† Email address for correspondence: tiron@kaist.ac.kr

https://doi.org/10.1017/S0022112010004891 Published online by Cambridge University Press

such a system have been developed and analysed extensively. In particular, asymptotic models that take advantage of typical long horizontal scale of the motion with respect to the widths of the fluid layers are notably much easier to study than their full Euler counterparts. For instance, the two-layer strongly nonlinear model for long waves of arbitrary amplitude described by Miyata (1985) and Choi & Camassa (1999) reduces the full Euler system of partial differential equations to a system of evolution equations for interface position, layer mean velocities and pressure at the interface, which are clearly more amenable to analytical investigations (as shown, for instance, by the closed-form solution for solitary waves). As the thickness of the pycnocline increases, two-layer models can be expected to offer increasingly poor approximations. In particular, the choice of corresponding two-layer parameters becomes unclear. Various simplified models that take into consideration the presence of a pycnocline of finite width have been studied (e.g. intermediate layer of constant density, Rusås 2001, Rusås & Grue 2002; or linear stratification, Fructus & Grue 2004, Fructus *et al.* 2009). However, studying time evolution and determining stationary solutions in the framework of such continuous stratification models is substantially more costly than the equivalent analysis using two-layer models. This is particularly relevant for asymptotic models of long waves, which can sometimes even admit analytic solutions in terms of tabulated functions.

Motivated by the relative ease of use of two-layer models and the analytical insight that they provide, in the present paper we extend the two-layer approximation to smooth density stratifications with a single finite-width pycnocline. We assume the fluid to be inviscid, incompressible and non-diffusive. Furthermore, we confine the upper surface by a rigid lid. We remark that the rigid-lid approximation is justified for the typical (small) density variations in oceanic applications, as internal waves under this assumption effectively decouple from their surface counterparts (see e.g. Lamb 1932) for most situations of interest. Our study shows that two-layer models can be successfully extended to account for rather large pycnocline thicknesses, provided the three parameters that comprise the model are judiciously chosen. In particular, we show that a selection criterion based on the conservation laws and dispersion relation for infinitesimal waves supported by the quiescent state offers accurate results in a broad range of single-pycnocline set-ups.

This paper is organized as follows. In § 2, we discuss strategies for constructing two-layer approximations for an arbitrary continuous stratification. In § 3, we test these strategies by comparing their performance with the (mathematically) simplest solutions for stratification and velocity shear of the full Euler continuously stratified system, respectively, those which arise in the limit of infinitesimal amplitude waves and those which arise in the opposite maximum amplitude limit of the so-called conjugate states. As is well known (e.g. Lamb & Wan 1998), the far-field stratification and shear for the latter solutions can be viewed as approximating that of the limiting case of internal solitary waves near their maximum amplitude regimes (at the largest displacement of density isolines location). Unlike solitary waves, however, this far-field state can be obtained by a simple one-dimensional nonlinear eigenvalue problem. We explore the range of pycnocline thicknesses for which the proposed models furnish reasonable estimates. In § 3.4, we further validate our strategy by comparing solitary-wave solutions of Euler equations in continuous stratification (obtained by a refined version of the fixed-point iteration algorithm of Turkington, Eydeland & Wang 1991 described in detail by Tiron 2009) with those of the strongly nonlinear long-wave model (Choi & Camassa 1999), which are available in closed form. Finally, in § 4 we construct a model capable of approximating local fluid velocities pointwise (as

https://doi.org/10.1017/S0022112010004891 Published online by Cambridge University Press

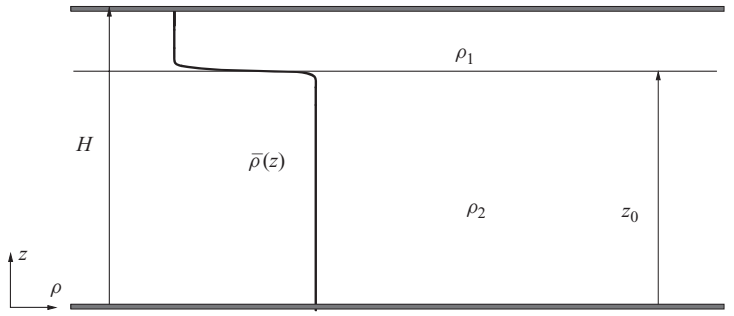


FIGURE 1. A schematic diagram of the two-layer system and its continuous stratification counterpart with our main notation.

opposed to layer-averages) everywhere in the fluid domain, based on the two-layer long-wave optimal strategy and incompressibility.

2. Model

Let $\overline{\rho}(z)$ denote a continuous density stratification for which we aim to determine an equivalent two-layer system. The two-layer system is fully determined by specifying three quantities: the height of the bottom layer, z_0, and the densities in each layer (ρ_1 upper, ρ_2 bottom) – see figure 1 for the notation. Hence, in general, one needs three criteria to match a two-layer model with a given continuous stratification. Dispersion is a fundamental aspect of wave motion in stratified fluids, and thus provides a natural criterion for selection of a two-layer system which would correctly capture wave dynamics in continuous stratification. The most significant physical quantity that characterizes dispersion in both two-layer and continuously stratified systems is the speed of waves of infinitesimal amplitude and infinite wavelength – the linearized long-wave speed.

The linearized long-wave speed for continuous stratification corresponds to the first eigenmode (baroclinic mode) of the linearized Euler equations. Assuming sinusoidal waves propagating in the horizontal direction x, the streamfunction can be expressed as $\psi(x, z, t) = F(z)\mathrm{e}^{\mathrm{i}k(x-ct)}$, with c being the phase speed of the wave, whereas k is the wavenumber. Upon linearization, a Sturm–Liouville eigenvalue problem is obtained for the amplitude $F(z)$ (Yih 1969; Love 1891), which in the limit $k \to 0$ is

$$F'' - \frac{N(z)^2}{g}F' + \frac{N(z)^2}{c^2}F = 0, \tag{2.1}$$

with $N(z) \equiv \sqrt{-\overline{\rho}'g/\overline{\rho}}$ being the Brunt–Väisälä frequency. The boundary conditions (slip at the top and bottom walls) are $F(0) = F(H) = 0$. The first eigenvalue of (2.1) gives the linearized long-wave speed (which is denoted by c_0^{cont}). In contrast with the case of continuous stratification, where the linearized speed requires the solution of a differential eigenvalue problem, the linearized long-wave speed for a two-layer system (Lamb 1932) with height of the bottom layer z_0, total height H and densities ρ_1, ρ_2 always admits an explicit relation

$$c_0^{two\ layers} = \sqrt{\frac{gz_0(H-z_0)(\rho_2-\rho_1)}{\rho_1 z_0 + \rho_2(H-z_0)}}. \tag{2.2}$$

https://doi.org/10.1017/S0022112010004891 Published online by Cambridge University Press

Other relevant physical quantities that characterize a stratified configuration in a quiescent state are the masses and potential energies of the two layers. In the following, we define functions representing differences between the quantities that characterize the continuous stratification and the two-layer configuration (mass in each layer, respectively potential energies in each layer):

$$f_1(z_0, \rho_1) \equiv \rho_1\ (H - z_0) - \int_{z_0}^{H} \overline{\rho}(z)\,\mathrm{d}z = \rho_1\ (H - z_0) + r(z_0) - \overline{r}, \tag{2.3}$$

$$f_2(z_0, \rho_2) \equiv \rho_2 z_0 - \int_{0}^{z_0} \overline{\rho}(z)\,\mathrm{d}z = \rho_2 z_0 - r(z_0), \tag{2.4}$$

$$f_3(z_0, \rho_1) \equiv \frac{\rho_1}{2}\left(H^2 - z_0^2\right) - \int_{z_0}^{H} z\overline{\rho}(z)\,\mathrm{d}z = \frac{\rho_1}{2}\left(H^2 - z_0^2\right) + W(z_0) - \overline{W}, \tag{2.5}$$

$$f_4(z_0, \rho_2) \equiv \frac{\rho_2}{2} z_0^2 - \int_{0}^{z_0} \overline{\rho}(z) z\,\mathrm{d}z = \frac{\rho_2}{2} z_0^2 - W(z_0), \tag{2.6}$$

where

$$r(z) \equiv \int_0^z \overline{\rho}(\xi)\,\mathrm{d}\xi, \quad W(z) \equiv \int_0^z z\overline{\rho}(\xi)\,\mathrm{d}\xi, \tag{2.7}$$

and $\overline{r} = r(H)$ is the total cross-section mass for the continuous stratification, whereas $g\overline{W} = gW(H)$ is the total cross-section potential energy for the continuous stratification.

Based on these quantities, there are multiple ways of prescribing effective two-layer models matched to a given continuum. Given that the equivalent two-layer system should accurately capture small-amplitude motion, we impose that the linearized speed be matched exactly. This allows elimination of one of the unknowns – for instance ρ_2 in favour of ρ_1 and z_0. Let $h_0 \equiv (c_0^{cont})^2/g$. From (2.2) we obtain

$$\rho_2(z_0, \rho_1) = \frac{(z_0 - h_0 - H) z_0 \rho_1}{(H - z_0)(h_0 - z_0)}\,. \tag{2.8}$$

We thus rewrite the functions (2.3)–(2.6) as

$$f_1(z_0, \rho_1) = \rho_1(H - z_0) + r(z_0) - \overline{r}, \tag{2.9}$$

$$f_2(z_0, \rho_1) = \rho_1 \frac{(z_0 - H - h_0) z_0^2}{(H - z_0)(h_0 - z_0)} - r(z_0), \tag{2.10}$$

$$f_3(z_0, \rho_1) = \frac{\rho_1}{2}\left(H^2 - z_0^2\right) + W(z_0) - \overline{W}, \tag{2.11}$$

$$f_4(z_0, \rho_1) = \frac{\rho_1}{2} \frac{(z_0 - H - h_0) z_0^3}{(H - z_0)(h_0 - z_0)} - W(z_0). \tag{2.12}$$

Next, having imposed the constraint of matched linearized speed, we investigate three different matching strategies: (i) mass in each layer, (ii) potential energy in each layer and (iii) least-squares fit for masses and energies in the two layers. In all three cases, we reduce the determination of the equivalent two-layer system problem to a nonlinear equation for the position of the interface z_0 (the width of the bottom layer). In most cases, this nonlinear equation has multiple solutions. In § 3 we will present prescriptions for selecting only one of the roots in each instance, in the context of a specific density stratification.

https://doi.org/10.1017/S0022112010004891 Published online by Cambridge University Press

2.1. *Matched mass in each layer*

Matching mass in each layer amounts to solving the nonlinear system of equations $f_1(z_0, \rho_1) = 0$ and $f_2(z_0, \rho_1) = 0$ (f_1, f_2 given by (2.9) and (2.10)) in the unknowns z_0, ρ_1. By adding the two equations, we can express ρ_1 in terms of z_0 as

$$\rho_1 = \frac{(H - z_0)(h_0 - z_0)\overline{r}}{H\left(z_0^2 - (H + 2h_0)z_0 + Hh_0\right)}. \tag{2.13}$$

Substituting this expression in the second equation $f_2(z_0, \rho_1) = 0$ yields a single equation in z_0,

$$F_1(z_0) \equiv \frac{(z_0 - h_0 - H)z_0^2\overline{r}}{H\left(z_0^2 - (H + 2h_0)z_0 + Hh_0\right)} - r(z_0) = 0. \tag{2.14}$$

Note that $z_0 = H$ is a solution.

2.2. *Matched potential energy in each layer*

We need to solve the nonlinear system of equations $f_3(z_0, \rho_1) = 0$ and $f_4(z_0, \rho_1) = 0$ (f_3, f_4 given by (2.11) and (2.12)) in the unknowns z_0, ρ_1. Adding the two equations yields

$$\rho_1 = \frac{2(H - z_0)(z_0 - h_0)\overline{W}}{H\left(H^2h_0 - H(H + h_0)z_0 + (H - h_0)z_0^2\right)}. \tag{2.15}$$

Substituting this expression in the second equation $f_4(z_0, \rho_1) = 0$ gives a single equation in z_0,

$$F_2(z_0) \equiv \frac{(z_0 - h_0 - H)z_0^3\overline{W}}{H\left(H^2h_0 - H(H + h_0)z_0 + (H - h_0)z_0^2\right)} - W(z_0) = 0. \tag{2.16}$$

Note that $z_0 = H$, $z_0 = 0$ are solutions.

2.3. *Least-squares fit for potential energies and masses*

We define the residue function

$$S(z_0, \rho_1) = \frac{f_1^2(z_0, \rho_1) + f_2^2(z_0, \rho_1)}{2r^2} + \frac{f_3^2(z_0, \rho_1) + f_4^2(z_0, \rho_1)}{2\overline{W}^2}. \tag{2.17}$$

In order to minimize the residual S, we determine the critical points, thus solving the system

$$\frac{\partial S}{\partial z_0}(z_0, \rho_1) = 0, \quad \frac{\partial S}{\partial \rho_1}(z_0, \rho_1) = 0, \tag{2.18}$$

and select the local minima. (Relations for the partial derivatives of $f_1(z_0, \rho_1)$ – $f_4(z_0, \rho_1)$ are reported explicitly in the Appendix.) In order to solve the system (2.18), we first solve the two corresponding root-finding problems in ρ_1 for the entire range $z_0 \in (0, H)$. Usually, we obtain several branches for both roots from which we select the branches that admit a common solution (intersection) – say $\rho_1^{(1)}(z_0)$ and $\rho_1^{(2)}(z_0)$. We define

$$F_3(z_0) = \rho_1^{(1)}(z_0) - \rho_1^{(2)}(z_0). \tag{2.19}$$

The roots of the above equation determine the critical points of the residual, from which we will select the global minima.

https://doi.org/10.1017/S0022112010004891 Published online by Cambridge University Press

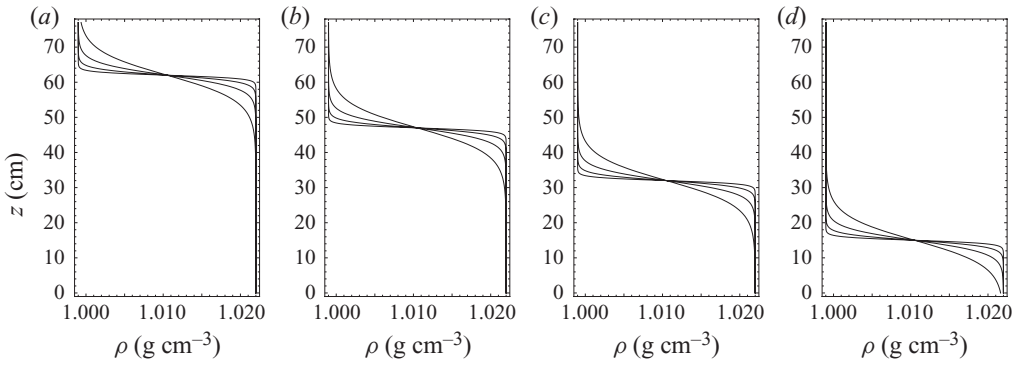


FIGURE 2. Density stratifications analysed in §§ 3 and 4, corresponding to the general stratification (3.1), for the position of the inflection point z_p at (*a*) 62, (*b*) 47, (*c*) 32 and (*d*) 17 cm and for the widths of the pycnocline of 2, 4, 8 and 16 cm, respectively.

3. Validation studies

The strategy outlined above can be expected to suffer from several limitations, which can be anticipated to become more prominent as the extra degrees of freedom of the continuously stratified fluids with respect to two-layer approximations become dynamically accessible. The next section will focus on some of these limitations and diagnostics to quantify them.

3.1. *Density stratification and resulting two-layer approximations*

In this section, we use as benchmark for validation the (smooth) antisymmetric density stratification

$$\overline{\rho}(z) = \rho_{min} + \frac{\rho_{max} - \rho_{min}}{2}(1 + \tanh[\alpha(z_p - z)]), \tag{3.1}$$

where ρ_{min}, ρ_{max} are the densities below and above the pycnocline (unless the pycnocline is close to the upper or lower vertical boundaries), z_p is the location of the inflection point (the centre) of the density stratification, and α is a parameter inversely proportional to the thickness of the pycnocline. We define the thickness of the pycnocline d, the distance between the points of 10 % and 90 % of the total density variation, i.e. the vertical locations in the density stratification corresponding to $\rho_{min} + 0.1\Delta\rho$ and $\rho_{max} - 0.1\Delta\rho$, respectively. Note that $\overline{\rho}(z_p) = \rho_{av} \equiv 1/2(\rho_{min} + \rho_{max})$. We fix the densities $\rho_{min} = 0.999\,\mathrm{g\,cm^{-3}}$, $\rho_{max} = 1.022\,\mathrm{g\,cm^{-3}}$ and the total height of the fluid column $H = 77\,\mathrm{cm}$, chosen to coincide with the corresponding physical parameters reported by Grue *et al.* (1999) in their experiments (most of which have been performed with a relatively thin pycnocline of ≈2 cm, with the centre of the pycnocline of the undisturbed configuration located at 62 cm). In the present study, we aim at monitoring the effectiveness of the matching strategy for various relative thicknesses of the intermediate layer, with respect to the widths of the two layers situated above and below the pycnocline. Thus, we study the two-parameter family of the density profiles (3.1) in the parameters d and z_p. We consider four widths and positions of the pycnocline: 2, 4, 8 and 16 cm and 62, 47, 32 and 17 cm, respectively; see figure 2 for plots of the corresponding density profiles. We note that stratifications in figure 2(*a*, *b*) support solitary waves of depression whereas those in figure 2(*c*, *d*) support solitary waves of elevation, as evidenced in § 3.3.

https://doi.org/10.1017/S0022112010004891 Published online by Cambridge University Press

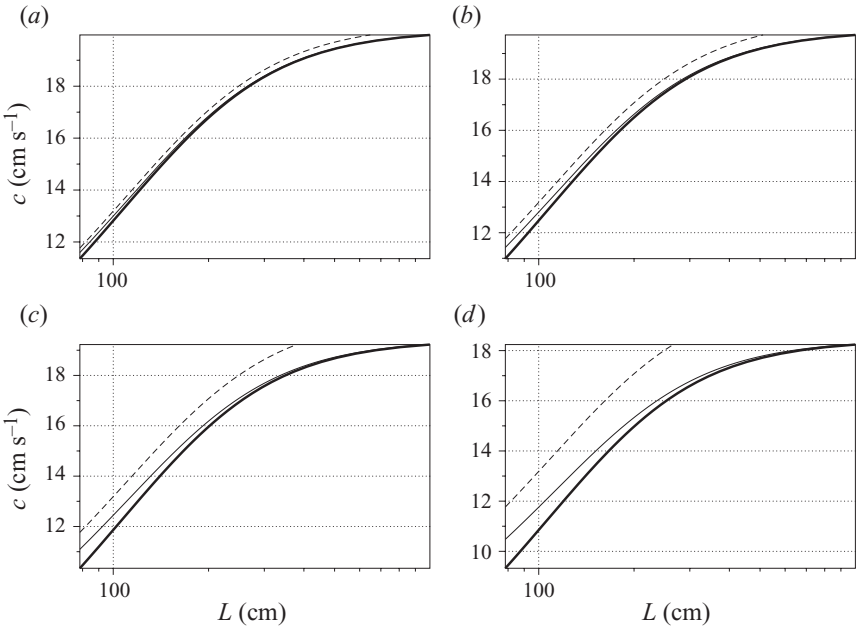


FIGURE 3. Dispersion relation for infinitesimal waves (c, speed as a function of L, wavelength). Lines: thick line, continuous stratification; dashed line, regular two-layer approximation; thin line, optimal two-layer approximation. The width of the pycnocline d is (a) 2 cm, (b) 4 cm, (c) 8 cm and (d) 16 cm, whereas the inflection point of the density stratification is located at $z_p = 32$ cm.

By matching either the masses or potential energies in each layer, the corresponding nonlinear equation for the height of the bottom layer z_0 has two real solutions (besides $z_0 = H$ for the matched masses strategy, and $z_0 = 0$, H for matched potential energies). We select the root closest to the inflection point of the density profile z_p (which will translate to a better prediction for the speed of the conjugate states, described in the following section).

By using the third matching strategy we obtain three roots. In this instance, we select the root corresponding to the global minimum, which for the stratifications analysed in this section corresponds to the root closest to the position of the inflection point of the density stratification z_p.

3.2. *Dispersion*

We first assess how accurately the effective two-layer models we have obtained capture the propagation of waves of infinitesimal amplitude and finite wavenumber. In figure 3, we compare the dispersion relation for the continuous density stratification $c = c(k)$ ($L = 2\pi/k$ wavelength, c phase speed) with that of the two-layer system. The former can be easily computed by solving the Sturm–Liouville problem (2.1) with zero boundary conditions, via a standard shooting method, while the latter is known explicitly to be

$$c(k) = k\sqrt{\frac{g(\rho_2 - \rho_1)}{\rho_1 \coth(h_1 k) + \rho_2 \coth(h_2 k)}}, \tag{3.2}$$

see Lamb (1932). We note that the three matching strategies yield very similar predictions of the dispersion relation; thus in figure 3 we depict only the effective two-layer model based on least-squares fit of the masses and potential energies. Notice that

https://doi.org/10.1017/S0022112010004891 Published online by Cambridge University Press

for wavelengths comparable to the total height of the fluid H, the effective two-layer model fails to capture the dispersion accurately in the continuous stratification, this effect being enhanced by increasing the pycnocline width d. However, its prediction is always superior to that of the regular two-layer model. We also point out that the agreement is excellent for $L/H > 1$; hence, these strategies can be used in conjunction with asymptotic models for long-wave motion, such as those developed by Choi & Camassa (1999).

3.3. *Conjugate states*

Euler equations in two-layer systems admit front solutions (internal bore solutions), which represent an upper bound for the amplitude of internal solitary waves. As solitary waves approach this limit, they develop long flat crests and/or troughs. The uniform flow at the extrema of such flat waves is said to be 'conjugate' to the upstream flow. Note that this upper bound and the speed of propagation are predicted exactly by the long-wave, strongly nonlinear model proposed by Miyata (1988) and Choi & Camassa (1999). Conjugate flows exist for any combination of density ratios $\rho_r = \rho_1/\rho_2$ of the two layers and depth ratios $h_r = h_1/h_2$, except when the depth ratio becomes critical $h_c = \sqrt{\rho_r}$.

Similar analytical predictions on the existence of internal bore solutions in the case of continuously stratified flows are not easily available. In fact, there exist (stable) density stratifications that do not seem to support conjugate flows, as revealed by a series of numerical investigations (Tung, Chan & Kubota 1982; Lamb & Wan 1998). Lamb & Wan (1998) have derived a numerical method for determining conjugate flows for arbitrary stratifications. By imposing conservation of mass, horizontal momentum and energy, they reduced the Euler equations to a nonlinear boundary value problem for the isopycnal displacement $\eta(z)$, with the speed of propagation as the eigenvalue. Furthermore, the density stratification (3.1) has been extensively analysed in these references, and shown to admit conjugate flow solutions except for a critical depth ratio z_c, in perfect analogy with two-layer systems.

In the light of these results, we next use conjugate states to test our effective two-layer models, both because these solutions of Euler equations can be computed accurately and inexpensively and because by being extreme cases they seem to provide the most challenging test for the optimal criterion strategies. We conjecture that a continuous density stratification that does not admit conjugate states cannot be approximated reasonably by a two-layer system. This is indicated by finite-amplitude effects that cannot be correctly captured by two-layer systems, such as narrowing of solitary-wave solutions for increasing amplitude in such stratifications. Conversely, for a continuous stratification that admits conjugate states, the speed and amplitude of the bore solutions become relevant matching criteria.

Following the strategy outlined by Lamb & Wan (1998), we compute conjugate flows in continuous stratification (3.1) for the parameters z_p and d specified in the previous section, and compare with the two-layer predictions by using parameters ρ_1, ρ_2 and z_0 chosen via the three proposed matching strategies. Figure 4 illustrates the front speed dependence on the width of the pycnocline. We remark that better agreement is achieved in general by employing the third strategy (least-squares fit for masses and potential energy in each layer), except in the case $z_p = 32$ cm in figure 4(*c*). This particular depth is close to the critical depth of the continuous stratification, that is, the depth that does not support a conjugate state. One can estimate the critical depth by interpolating the maximum displacement of the conjugate states for various positions of the centre of the pycnocline z_p, and subsequently determine

https://doi.org/10.1017/S0022112010004891 Published online by Cambridge University Press

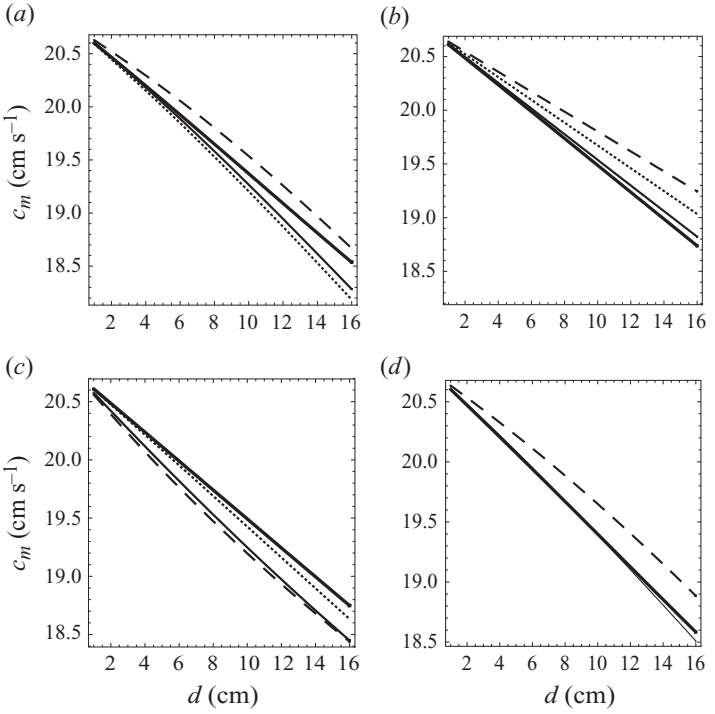


FIGURE 4. Conjugate states: speed dependence on the thinckness of the pycnocline. Thick solid line, speed corresponding to the conjugate state for stratifications (3.1) (with the inflection point of the density stratification located at (*a*) $z_p = 62$ cm, (*b*) $z_p = 47$ cm, (*c*) $z_p = 32$ cm and (*d*) $z_p = 17$ cm, respectively) as a function of the width of the pycnocline d; dotted line, the two-layer predictions with matched masses; dashed line, matched potential energies; thin solid line, least-squares fit for the masses and potential energy.

the depth for which the maximum displacement is zero. For our stratification, the critical depth ranges between 38.714 cm for the pycnocline thickness $d = 2$ cm and 38.645 cm for $d = 16$ cm. Given the broad applicability away from isolated critical depth degeneracies, from now on we will use the term 'optimal' to designate the model produced by our third strategy (based on both mass and potential energy) for defining effective two-layer parameters.

In figure 5, we compare the vertical displacement of the average density isoline with the displacement of the interface predicted by the two-layer model. Note that in the limit $d \to 0$, i.e. of the two-layer system, the interface displacement naturally reduces to the maximum amplitude wave value determined by the densities and depth ratios (see e.g. Choi & Camassa 1999). Note that the polarity of the conjugate states (and consequently that of the entire branch of solitary-wave solutions) is of depression in figures 5(*a*) and 5(*b*) and of elevation in figures 5(*c*) and 5(*d*), respectively.

We also display for comparison the vertical displacement of the density isolines for the continuous stratification corresponding to $\rho(x, z) = \overline{\rho}(z_0)$. Note that the displacement of these isolines is close to that of the average density profile for the entire range of pycnocline widths. On the basis of this observation, we can construct an estimate of the average density isoline position for the continuous stratification by simply translating the interface predicted by the optimal two-layer model $z = \zeta(x, t)$ in the vertical direction with $z_p - z_0$.

https://doi.org/10.1017/S0022112010004891 Published online by Cambridge University Press

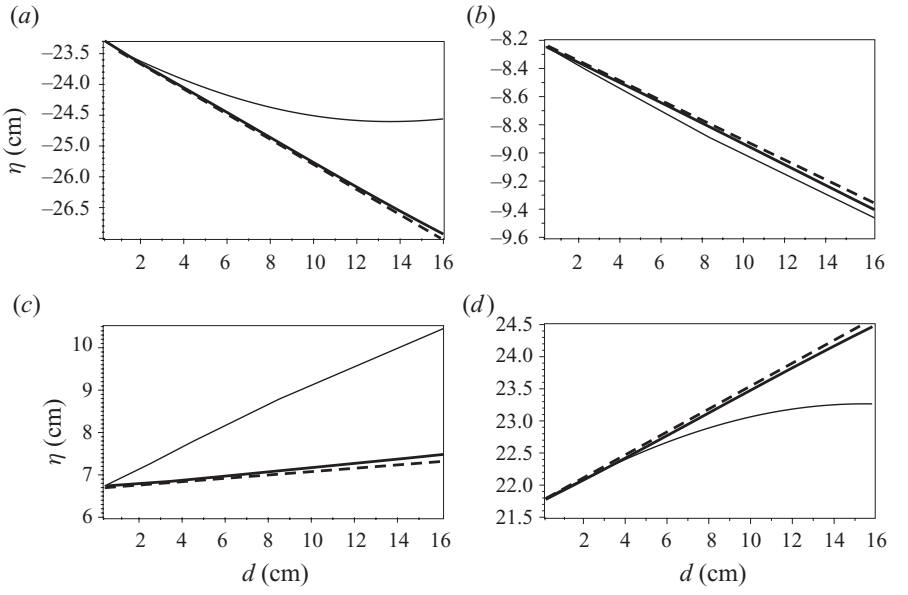


FIGURE 5. Conjugate states: displacement dependence on the thinckness of the pycnocline. Thick solid line, displacement of the average density isoline corresponding to the conjugate state for stratifications (3.1) (with the inflection point of the density stratification located at (*a*) $z_p = 62$ cm, (*b*) $z_p = 47$ cm, (*c*) $z_p = 32$ cm and (*d*) $z_p = 17$ cm, respectively) as a function of the width of the pycnocline d; dashed line, displacement of the density isoline $\rho(x, z) = \overline{\rho}(z_0)$ of the conjugate states in the continuous stratifications, with $\overline{\rho}(z)$ being the background stratification and z_0 being the interface position for the optimal two-layer system; thin solid line, displacement of the interface corresponding to the conjugate state of the optimal two-layer system.

3.4. *Solitary-wave solutions*

We now test the performance of the optimal two-layer approximation described in the previous section in the case of solitary-wave solutions, which is perhaps the solution class of most interest in field applications. As remarked above, compared to conjugate states this class of solutions may in general be expected to constitute a less demanding test for optimal two-layer models, but exceptions can of course arise. We further remark that comparisons with experiments of Grue *et al.* (1999) have been reported by Camassa *et al.* (2006) for solitary-wave solutions of the simple (non-optimal) two-layer model; both the horizontal velocity shear profile at the maximal displacement of the pycnocline and the wave profiles have been found to compare favourably with the data. Nonetheless, errors inherent in the non-optimal choice become evident and substantial in the region around the inflection points of the wave isopycnal profiles, but unfortunately data from the experiment in these regions are not available. The lack of data necessary for a thorough validation can be partially overcome by a comparison of simulations of the direct initial value problem of the experimental set-up in Grue *et al.* (1999). This validation has been performed and findings will be reported in a forthcoming paper (preliminarily reported in Tiron 2009).

In this section, we will compare fundamental properties of the waves (wave speed, shape, kinetic and potential energy) in continuous stratification (as solutions of full Euler system, using a variant of the algorithm constructed by Turkington *et al.* 1991 described in Tiron 2009, Appendix C) with properties of the waves in a two-layer

https://doi.org/10.1017/S0022112010004891 Published online by Cambridge University Press

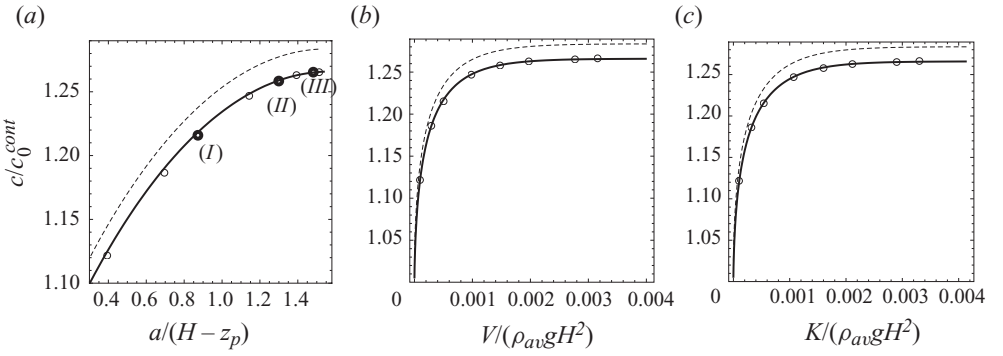


FIGURE 6. Properties of solitary-wave solutions for the density stratification (3.1) with $H = 77$ cm, the inflection point located at $z_p = 62$ cm and the thickness of the pycnocline $d = 2$ cm. (a) Speed versus the maximum displacement of the average density isoline. (b) Potential energy versus speed. (c) Kinetic energy versus speed. Circles, Euler solutions in continuous stratification; dashed line, regular two-layer; solid line, equivalent two-layer least squares for masses and potential energy in each layer (optimal two-layer model). ρ_{av} is the average density for the continuous stratification.

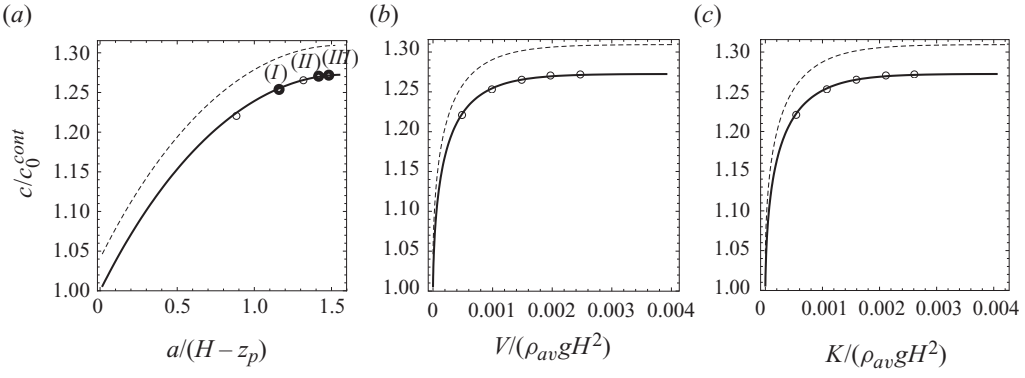


FIGURE 7. The same as figure 6, for the thickness of the pycnocline $d = 4$ cm.

system for which asymptotic quadrature expressions are available (see e.g. Miyata 1988; Choi & Camassa 1999). We consider the density stratifications in figure 2(a) (the centre of the pycnocline located at $z_p = 62$ cm and widths of the pycnocline ranging between 2 and 16 cm).

In figures 6–9, we show the amplitude, kinetic energy and potential energy as functions of the speed of the solitary-wave solutions in continuous stratification versus the two-layer approximations (see Camassa *et al.* 2010 for explicit expressions). (For the continuous stratification we take the amplitude as defined by the maximum displacement of the average density isoline, whereas for the two-layer model we take the absolute value of the signed amplitude used by Camassa *et al.* 2010.) The regular two-layer model overpredicts the speed of propagation of the solutions in continuous stratification, even for narrow pycnoclines, as evidenced in figure 6(a). Note the excellent agreement of the integral properties (kinetic and potential energy) as predicted by the optimal two-layer model with the properties of the solutions in continuous stratification. An accurate estimate of the potential energy is particularly useful in the context of determining specific solitary-wave solutions (e.g. waves of

https://doi.org/10.1017/S0022112010004891 Published online by Cambridge University Press

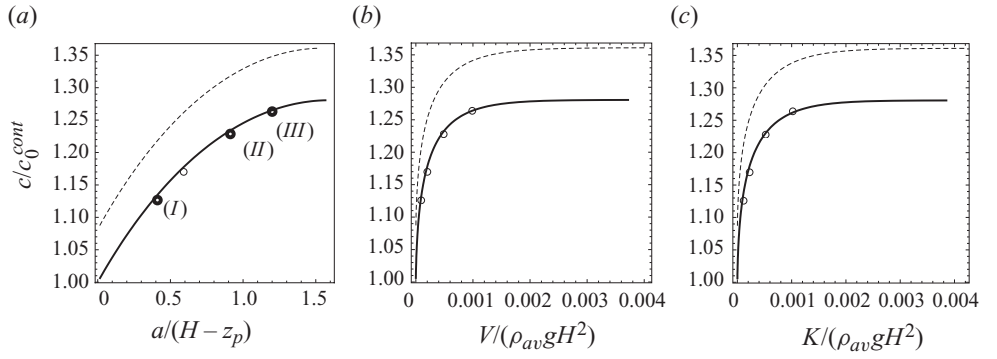


FIGURE 8. The same as figure 6, for the thickness of the pycnocline $d = 8$ cm.

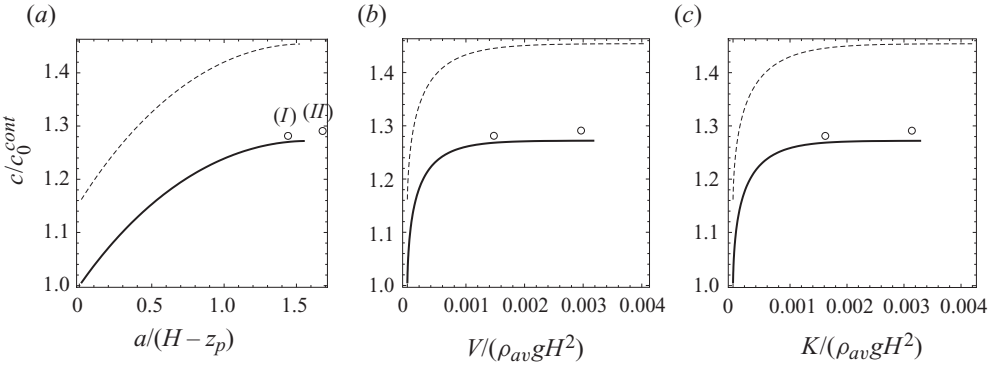


FIGURE 9. The same as figure 6, for the thickness of the pycnocline $d = 16$ cm.

prescribed speed and amplitude) using the algorithm proposed by Turkington *et al.* (1991), since the potential energy is an input of the corresponding iterative scheme.

In figures 10, 12, 14 and 16 we display the density field for solitary-wave solutions of Euler equations in continuous stratification corresponding to the points marked in subfigure (*a*) in each of figures 6–9, whereas in figures 11, 13, 15 and 17 we compare wave shapes corresponding to these solutions with the two-layer approximations. All density fields are computed by our version of the iterative scheme with periodic boundary conditions in the domain shown, which corresponds to the physical horizontal dimension of 12.32 m. The aspect ratio for all the density plots is altered by rescaling (doubling) the vertical scale with respect to the horizontal scale. By comparing with waves of the same amplitude obtained with the two-layer models, we observe that the optimal two-layer approximation is equivalent to that of the regular two-layer model, except in the large-amplitude regime; see figures 11(*I.a–III.a*), 13(*I.a–III.a*), 15(*I.a–III.a*) and 17(*I.a*). When matching for speed, we notice a much better performance of the optimal two-layer model compared with its regular counterpart.

We remark that all solitary-wave solutions in continuous stratification exhibit the behaviour referenced in § 3.3, that is, flattening for increasing amplitude; see figures 10, 12, 14 and 16. Note that for large pycnocline thicknesses such as in figure 16, the maximum amplitude allowed by the optimal two-layer model is smaller than that supported by the full continuously stratified Euler theory, as can be seen in figure 5 for large d, and so the corresponding wave profile for matched speed is missing in

https://doi.org/10.1017/S0022112010004891 Published online by Cambridge University Press

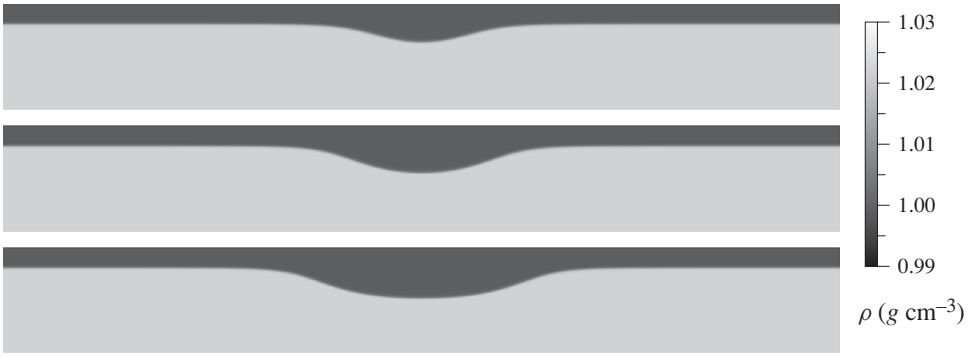


FIGURE 10. Density field for solitary-wave solutions corresponding to the points marked in figure 6(*a*) ($d = 2$ cm).

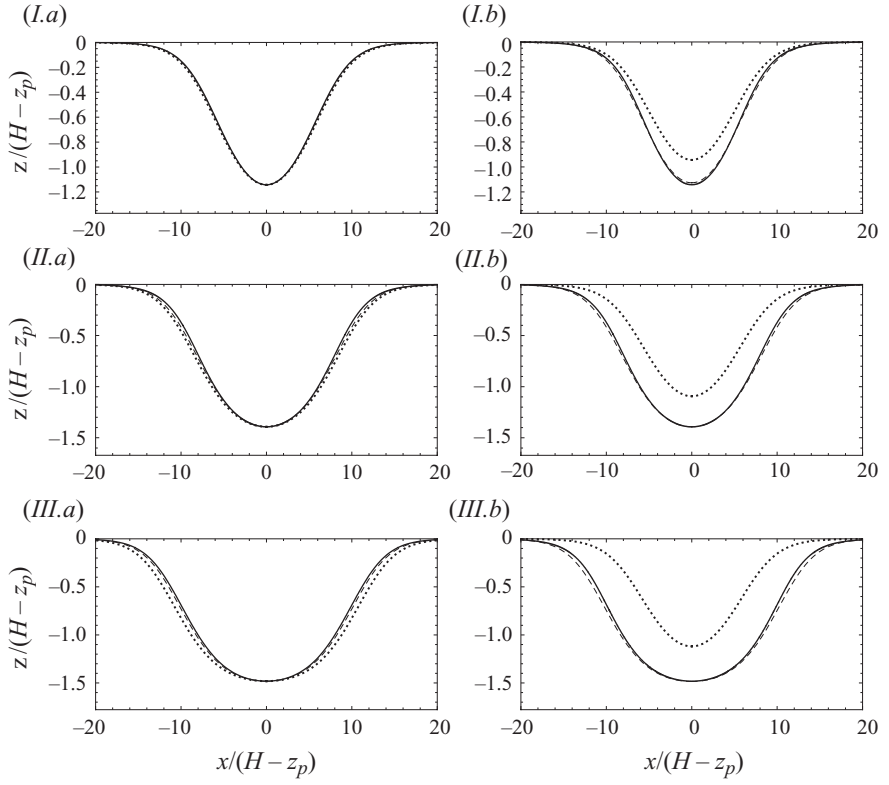


FIGURE 11. Comparison between the wave profiles of solitary-wave solutions in continuous stratification (corresponding to the points marked in figure 6*a*) and the two-layer approximations. (*I.a–III.a*) Matched amplitude and (*I.b–III.b*) matched speed. Lines: solid line, Euler solutions; dotted line, regular two-layer model; dashed line, optimal two-layer model.

figure 17(*I.b*). In particular, for $d = 16$ cm, we have computed a solitary-wave solution for the continuously stratified Euler system with an amplitude larger than the maximal amplitude predicted by the optimized two-layer model; see point (*II*) in figure 9(*a*). Thus, in this instance, we cannot compare wave shapes for matched amplitude.

https://doi.org/10.1017/S0022112010004891 Published online by Cambridge University Press



FIGURE 12. Density field for solitary-wave solutions corresponding to the points marked in figure 7(*a*) ($d = 4$ cm).

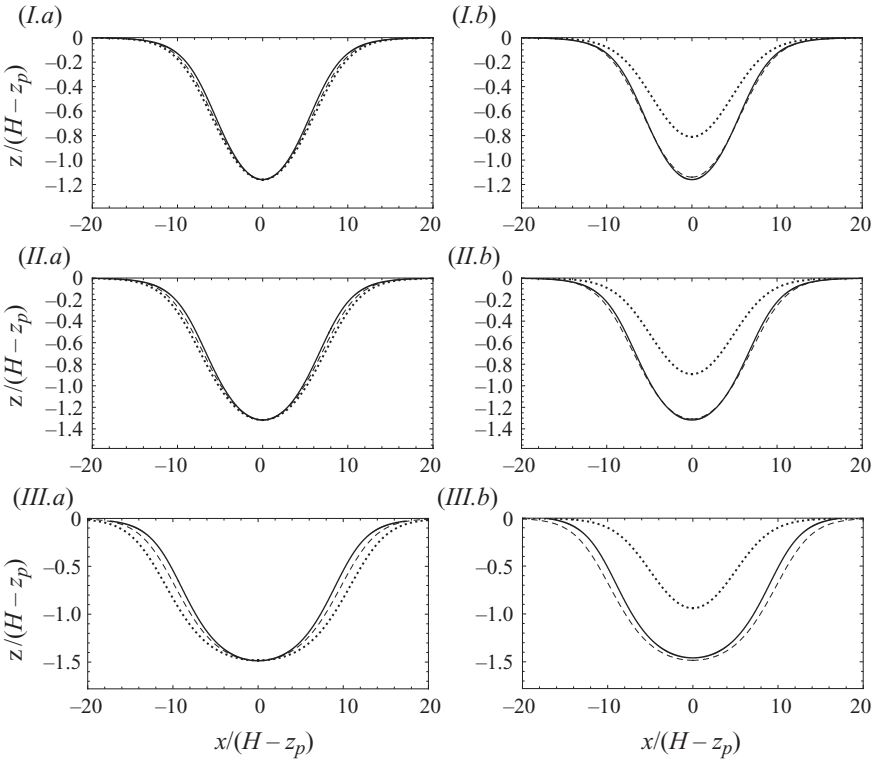


FIGURE 13. The same as figure 11, corresponding to the points marked in figure 7(*a*). (*I.a–III.a*) Matched amplitude and (*I.b–III.b*) matched speed. Lines: solid line, Euler solutions; dotted line, regular two-layer model; dashed line, optimal two-layer model.

Nonetheless, properties of smaller amplitude waves even for this large pycnocline configuration are still well captured by the optimized two-layer model (see figure 9).

4. Reconstruction of the velocity field from the two-layer approximation

Having looked into wave quantities in the previous section, we next proceed to focus on fluid parcel quantities such as the velocity field induced by long-wave motion in a continuously stratified fluid. As seen above, the optimal selection of parameters for the

https://doi.org/10.1017/S0022112010004891 Published online by Cambridge University Press



FIGURE 14. Density field for solitary-wave solutions corresponding to the points marked in figure 8(*a*) ($d = 8$ cm).

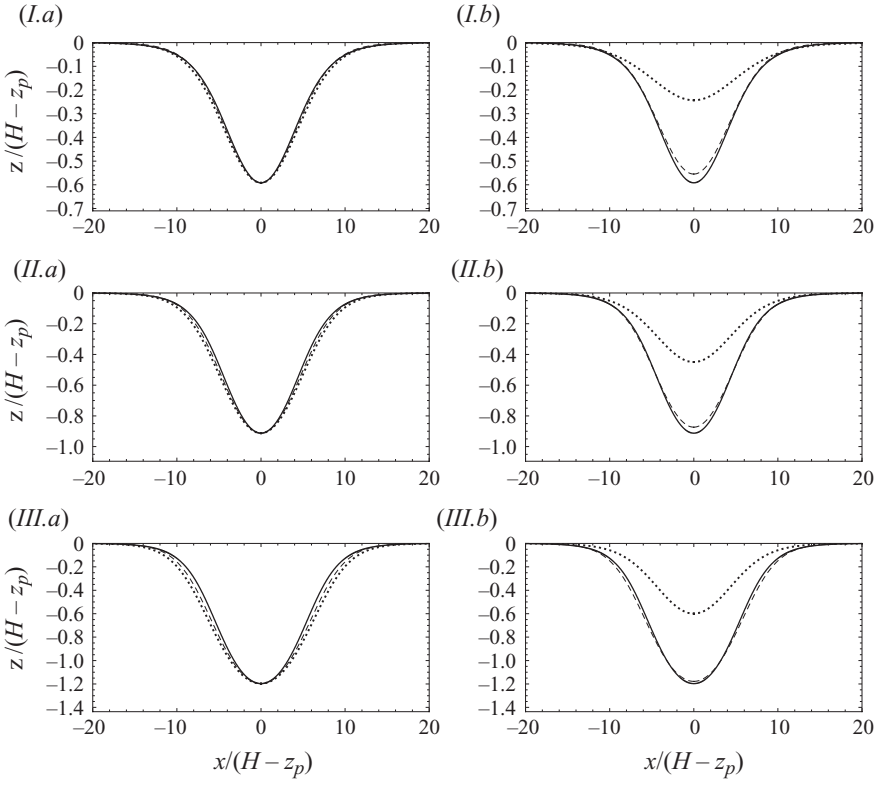


FIGURE 15. The same as figure 11, corresponding to the points marked in figure 8(*a*). (*I.a–III.a*) Matched amplitude and (*I.b–III.b*) matched speed. Lines: solid line, Euler solutions; dotted line, regular two-layer model; dashed line, optimal two-layer model.

two-layer system yields good estimates for the isopycnal displacement corresponding to the average density and for the speed of propagation. Local velocities can be estimated using the strongly nonlinear model (accurate to order $O(\epsilon^4)$ for long waves in a two-layer system, with the small parameter $\epsilon = H/L$ defined by the typical vertical

https://doi.org/10.1017/S0022112010004891 Published online by Cambridge University Press



FIGURE 16. Density field for solitary-wave solutions corresponding to the points in figure 9(*a*) ($d = 16$ cm).

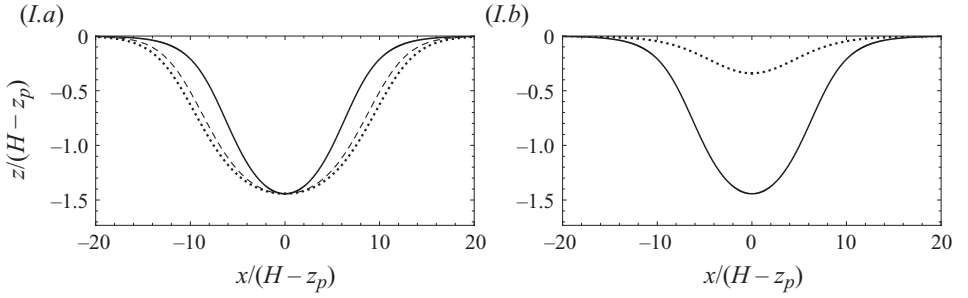


FIGURE 17. The same as figure 11, corresponding to the point marked (*I*) in figure 9(*a*). (*I.a*) matched amplitude and (*II.b*) matched speed. Lines: solid line, Euler solutions; dotted line, regular two-layer model; dashed line, optimal two-layer model. For this large pycnocline thickness, the continuously stratified Euler wave speed exceeds the maximal speed of the optimal model; thus, no corresponding wave profile appears in (*I.b*); similarly, for the second point marked (*II*) in figure 9(*a*) (corresponding to the second density plot in figure 16), the amplitude exceeds the maximal amplitude of the optimal two-layer model.

scale H and the horizontal scale L). However, when the thickness of the pycnocline is large, these estimates underpredict the fluid velocity, since they cannot capture the structure of the shear in the pycnocline region (the velocity predicted by the two-layer theory exhibits a jump across the interface). In the following, we include the effect of the finite pycnocline by assuming linear density stratification and shear in the pycnocline region and imposing volume conservation; we then reconstruct the velocity field from the isopycnal displacement and the speed of propagation predicted by the two-layer model. We restrict our attention to the case of waves of permanent form, propagating with constant speed c. Nonetheless, this analysis is extendable to time-dependent wave evolution, although in the time-dependent case, validation tests become more involved.

Let $\zeta(x, t)$ denote the displacement of the average density isoline, as predicted by the two-layer model; see figure 18 for a simple schematic diagram. For a stationary wave moving from left to right with constant speed c, we make the change of variable

$$X = x - ct, \tag{4.1}$$

and consider

$$\zeta(x, t) \equiv \zeta(X), \quad u(x, z, t) \equiv u(X, z), \quad w(x, z, t) \equiv w(X, z), \tag{4.2}$$

where u, w are the horizontal and vertical fluid velocities, respectively. We place the coordinate system at the level of the pycnocline centre of the background stratification $\overline{\rho}(z)$, which implies $\overline{\rho}(0) = \rho_{av}$. We approximate the background density profile in the

https://doi.org/10.1017/S0022112010004891 Published online by Cambridge University Press

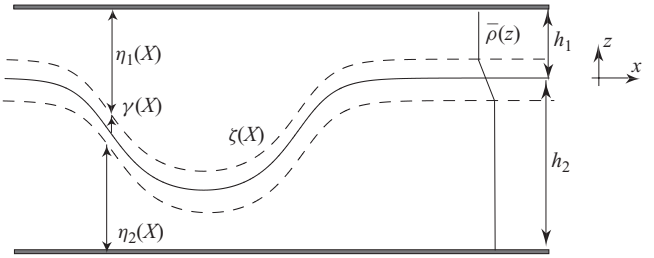


FIGURE 18. A schematic diagram of the three-layer system with our main notation.

intermediate layer by using a linear stratification that passes through the centre of the pycnocline and has the same slope as the continuous stratification in the quiescent state. The corresponding thickness of the quiescent state $2\widetilde{\gamma}$ is thus

$$2\widetilde{\gamma} = \frac{\rho_{min} - \rho_{max}}{2\overline{\rho}'(0)}. \tag{4.3}$$

Let $\gamma(X)$ denote half the thickness of the pycnocline at some location X, with $\gamma(X) \to \widetilde{\gamma}$ as $|X| \to \infty$. We allow the pycnocline thickness to vary in the horizontal direction; however, we assume that the variation is slow and also that the thickness is smaller than widths of any of the outer layers. Thus, we write the density field as

$$\rho(X,z) = \begin{cases} \dfrac{\rho_{min} - \rho_{max}}{2\gamma(X)} z + \dfrac{\rho_{min} + \rho_{max}}{2}, & \text{if } z \in [\zeta(X) - \gamma(X), \zeta(X) + \gamma(X)], \\ \rho_{min}, & \text{if } z \in [\zeta(X) + \gamma(X), h_1], \\ \rho_{max}, & \text{if } z \in [-h_2, \zeta(X) - \gamma(X)]. \end{cases} \tag{4.4}$$

We denote by $\eta_1(X)$ and $\eta_2(X)$ the widths of the two layers of constant densities,

$$\eta_1(X) \equiv h_1 - \zeta(X) - \gamma(X), \quad \eta_2(X) \equiv h_2 + \zeta(X) - \gamma(X). \tag{4.5}$$

Furthermore, we approximate the horizontal velocity in the pycnocline region $z \in [\zeta(X) - \gamma(X), \zeta(X) + \gamma(X)]$ with a linear profile

$$u_{pyc}(X,z) = \frac{u_1(X,\gamma(X)) - u_2(X,-\gamma(X))}{2\gamma(X)} z + \frac{u_1(X,\gamma(X)) + u_2(X,-\gamma(X))}{2}, \tag{4.6}$$

where $u_k(X,z)$, $k = 1, 2$ are the fluid velocities in each homogeneous density layer, and where we have imposed continuity of the horizontal velocity at the two interfaces. In the uniform density layers, assuming irrotationality, the local velocities can be reconstructed from the layer-averaged velocities

$$\overline{u}_k(X) \equiv \int_{[\eta_k]} u_k(X,z)\,\mathrm{d}z, \quad k = 1, 2, \tag{4.7}$$

by the same asymptotic relations derived by Camassa *et al.* (2006) for the two-layer models, which in turn can be related to the thickness γ by imposing volume conservation in the outer layers

$$(\overline{u}_k - c)\eta_k = -c(h_k - \widetilde{\gamma}), \quad k = 1, 2, \tag{4.8}$$

which implies

$$\overline{u}_k = c\left(1 - \frac{h_k - \widetilde{\gamma}}{\eta_k}\right), \quad k = 1, 2. \tag{4.9}$$

https://doi.org/10.1017/S0022112010004891 Published online by Cambridge University Press

Finally, by imposing conservation of volume for the intermediate layer, we obtain an equation involving only the thickness of the pycnocline $\gamma(X)$. In the following, we deduce this equation, as an algebraic equation in $\gamma(X)$, by taking advantage of the scaling $\gamma/H \equiv \delta \ll 1$. We introduce the scaled independent variables

$$X^* = \frac{X}{L}, \quad z^* = \frac{z}{H}, \tag{4.10}$$

and the scaled dependent variables

$$u_i^* = \frac{u_i}{U_0}, \quad \rho_i^* = \frac{\rho_i}{\rho_{av}}, \quad \delta\gamma^* = \frac{\gamma}{H}, \tag{4.11}$$

where U_0 is a reference horizontal fluid velocity (assumed to scale as $1/\epsilon$ with respect to the reference vertical velocity in long-wave theory).

The horizontal velocities in the constant density layers are (Camassa *et al.* 2006)

$$u_1^*(X^*, z^*) = \overline{u}_1^*(X^*) + \epsilon^2 \left(\frac{\eta_1^*(X^*)^2}{6} - \frac{(h_1^* - z^*)^2}{2} \right) \partial_{X^*}^2 \overline{u}_1^*(X^*) + O(\epsilon^4), \tag{4.12}$$

if $z^* \in [\zeta^*(X^*) + \delta\gamma^*(X^*), h_1^*]$, and

$$u_2^*(X^*, z^*) = \overline{u}_2^*(X^*) + \epsilon^2 \left(\frac{\eta_2^*(X^*)^2}{6} - \frac{(h_2^* + z^*)^2}{2} \right) \partial_{X^*}^2 \overline{u}_2^*(X^*) + O(\epsilon^4), \tag{4.13}$$

if $z^* \in [-h_2^*, \zeta^*(X^*) - \delta\gamma^*(X^*)]$, respectively. Using relation (4.9), the second derivative of the mean-layer velocities can be expressed as

$$\partial_{X^*}^2 \overline{u}_k^*(X^*) = c^* \left[\frac{(h_k^* - \delta\widetilde{\gamma}^*)\eta_k^{*\prime\prime}}{\eta_k^{*2}} - \frac{2(h_k^* - \delta\widetilde{\gamma}^*)\eta_k^{*\prime 2}}{\eta_k^{*3}} \right] = c^* \left[(-1)^k \frac{h_k^* \zeta^{*\prime\prime}}{\eta_k^{*2}} - \frac{2h_k^* \zeta^{*\prime 2}}{\eta_k^{*3}} \right] + O(\delta), \tag{4.14}$$

recalling definition (4.5) of the outer-layer widths.

By replacing (4.14) in (4.12)–(4.13) and discarding terms of order $O(\delta\epsilon^2)$, we thus obtain the following asymptotic relation for the horizontal shear in the layers of constant densities, rewritten in dimensional form:

$$u_k(X, z) = c \left[1 - \frac{h_k - \widetilde{\gamma}}{\eta_k} + \left(\frac{\eta_k^2}{6} - \frac{(h_k + (-1)^k z)^2}{2} \right) \left(\frac{(-1)^k h_k \zeta''}{\eta_k^2} - \frac{2h_k \zeta'^2}{\eta_k^3} \right) \right]. \tag{4.15}$$

Substituting the velocities at the two interfaces

$$u_k|_{\eta_k} = c \left[1 - \frac{h_k - \widetilde{\gamma}}{\eta_k} + h_k \left(\frac{(-1)^k \zeta''}{3} - \frac{2\zeta'^2}{\eta_k} \right) \right], \quad k = 1, 2, \tag{4.16}$$

in the formula for the inner-layer velocity (4.6) yields a relation for the shear in the pycnocline region, which depends algebraically on the unknown width $\gamma(X)$. Finally, imposing volume conservation in the inner layer

$$\int_{-\gamma(X)}^{\gamma(X)} (u_{pyc}(X, z) - c)\, \mathrm{d}z = -2c\widetilde{\gamma}, \tag{4.17}$$

we obtain an algebraic (cubic) equation for $\gamma(X)$, which can be solved for any fixed X location

$$\gamma \left[\frac{h_1 - \widetilde{\gamma}}{\eta_1} - h_1 \left(\frac{\zeta''}{3} + \frac{2\zeta'^2}{3\eta_1} \right) + \frac{h_2 - \widetilde{\gamma}}{\eta_2} + h_2 \left(\frac{\zeta''}{3} - \frac{2\zeta'^2}{3\eta_2} \right) \right] = 2\widetilde{\gamma}, \tag{4.18}$$

https://doi.org/10.1017/S0022112010004891 Published online by Cambridge University Press

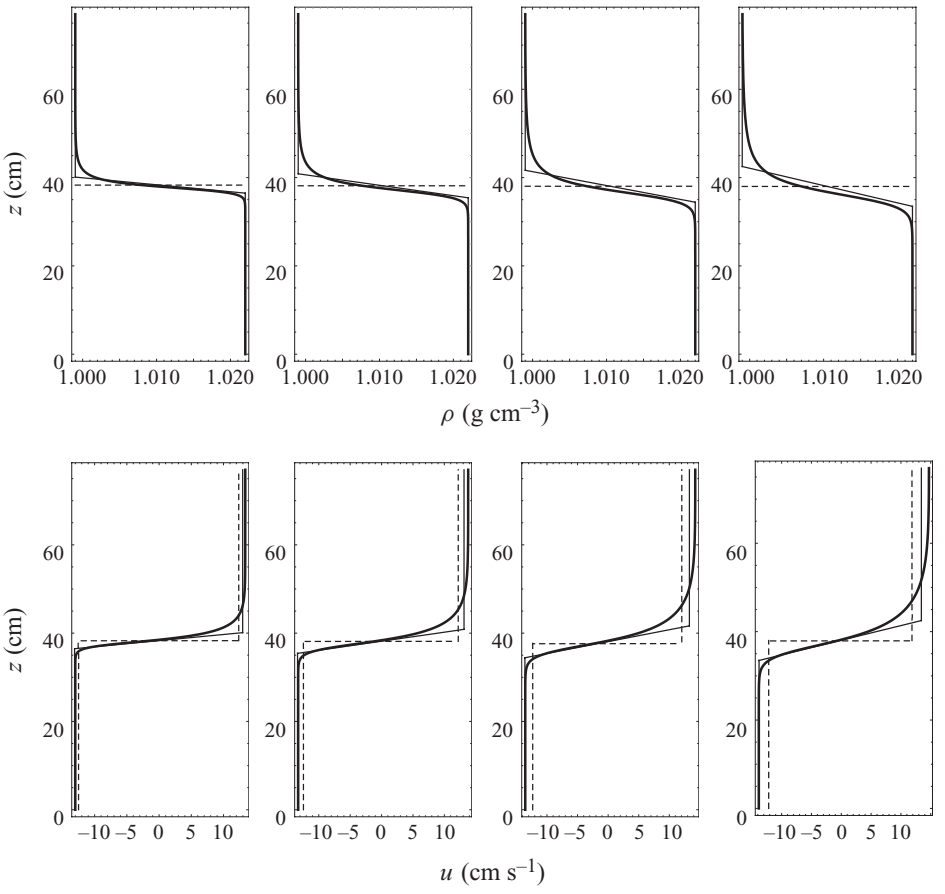


FIGURE 19. Density and horizontal shear for conjugate states in a stratification (3.1) with total depth of the fluid layer $H = 77\,\mathrm{cm}$, centre of the pycnocline located at $z_p = 62\,\mathrm{cm}$, densities in the outer layers $\rho_{min} = 0.999\,\mathrm{g\,cm^{-2}}$, $\rho_{max} = 1.022\,\mathrm{g\,cm^{-2}}$ and thickness of the pycnocline (distance between the vertical locations in the density stratification corresponding to $\rho_{min} + 0.1\Delta\rho$ and $\rho_{max} - 0.1\Delta\rho$, respectively) of 4, 6, 8 and 10 cm. Lines: thick solid line, Euler solution in continuous stratification; dashed line, prediction of the strongly nonlinear model for the optimized choice of parameters; thin solid line, predictions of the optimized two-layer model with correction that includes the presence of the finite-width pycnocline.

where we have suppressed all functional X-dependences for ease of notation. In figure 19, we present shear and density profiles for conjugate states for the stratification (3.1) (with $z_p = 62\,\mathrm{cm}$ and pycnocline widths ranging from $d = 4$ to $d = 10\,\mathrm{cm}$) constructed using the strategy described above. Note that when including the effect of the finite pycnocline, the agreement for the velocity between the smooth stratification case and its linear approximation degrades more visibly for the top layer with increasing effective thickness of the pycnocline (albeit while maintaining a superior agreement with respect to the strictly two-layer prediction throughout). Nonetheless, the maximum slope of the shear in the pycnocline region is very well captured.

Finally, in figure 20 we compare horizontal shear profiles for an internal solitary-wave solution in continuous stratification, at three horizontal locations along the wave profile, with the two-layer predictions. The horizontal velocity is computed with

https://doi.org/10.1017/S0022112010004891 Published online by Cambridge University Press

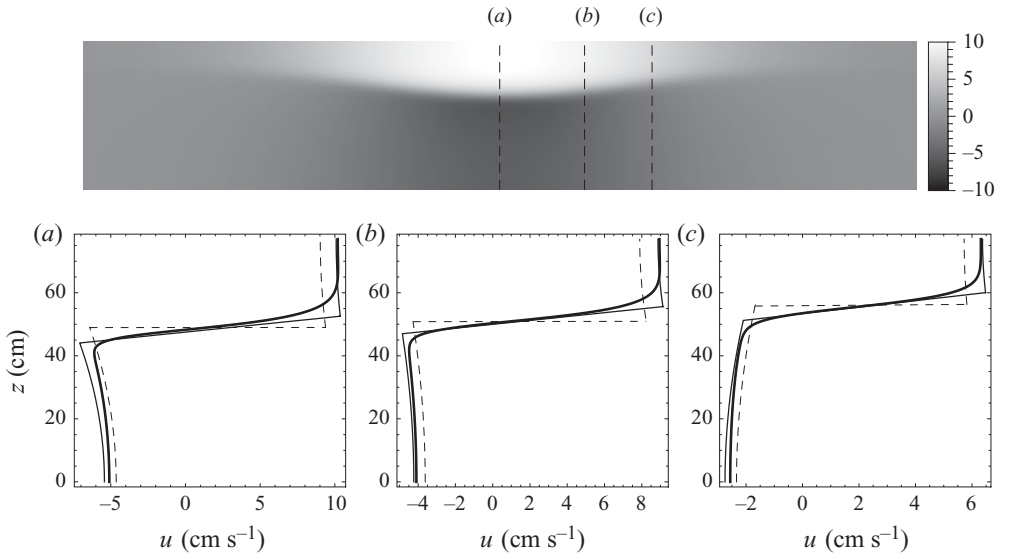


FIGURE 20. Horizontal shear for a solitary-wave solution in a stratification (3.1) (with total depth of the fluid layer $H = 77$ cm, centre of the pycnocline located at $z_p = 62$ cm, densities in the outer layers $\rho_{min} = 0.999\,\mathrm{g\,cm^{-3}}$, $\rho_{max} = 1.022\,\mathrm{g\,cm^{-3}}$ and thickness of the pycnocline of 8 cm) at (*a*) maximum displacement of the pycnocline, (*b*) a distance $X = 44$ cm from the maximum displacement and (*c*) $X = 79$ cm, respectively. Lines: thick solid line, Euler solution in continuous stratification; dashed line, prediction of the strongly nonlinear model for optimized choice of parameters; thin solid line, predictions of the optimized two-layer model with correction that includes the presence of the finite-width pycnocline.

the iterative scheme in a periodic domain of physical horizontal length 12.32 m, of which we show only the 4.26 m long portion (with no aspect ratio rescaling) centred at the pycnocline maximum displacement. As this figure demonstrates, the agreement between the intermediate linear stratification and the full Euler solution is remarkable even in this case of a relatively thick pycnocline.

5. Discussion

We have constructed a two-layer approximation for internal-wave dynamics in a smoothly stratified Euler fluid with one pycnocline. The simple three-parameter (top and bottom densities and quiescent-state interface position) choice of the two-layer model is optimized on the continuous stratification parameters by implementing a strategy that captures the speed of propagation of both dispersive waves and nonlinear solitary-wave solutions (including internal bores). We have tested this strategy on the extreme cases of the so-called conjugate state solutions for the continuously stratified fluid. For these states, we have found that our new strategy for choosing the optimal equivalent two-layer system approximates the isopycnal displacement of the centre of the pycnocline reasonably well, up to thicknesses comparable with the widths of the two layers, in fact well beyond what can be expected for a two-layer system. Integral properties of the motion, such as kinetic and potential energy, are also well predicted throughout these large thicknesses. We have further confirmed that these good agreement properties extend, even with improvements in most cases, to the solitary-wave solutions of the smoothly stratified Euler system obtained with a refined version of the algorithm by Turkington *et al.* (1991), by an extensive

https://doi.org/10.1017/S0022112010004891 Published online by Cambridge University Press

comparison across the parametric space of wave amplitudes, stratification thickness and pycnocline location. It is remarkable that this good agreement does not seem to require the choice of an equivalent two-layer model for continuous stratification tailored for solitary-wave propagation parameters as in Sakai & Redekopp (2007), at least for the stratification class we have tested.

Of course, local fluid properties, as opposed to global fluid properties such as wave speed or energy, of internal waves are also of great practical interest. For instance, Eulerian fluid velocities at different locations in the fluid are of interest for predicting the magnitude of fluid currents in experiments and field observations. By design, the two-layer model provides good estimates of layer-averaged velocities, but fails to describe the structure of the velocity field in the pycnocline region. However, we have found that it is possible to build further on the optimal two-layer model and produce accurate pointwise velocity approximations throughout the fluid domain. By a simple application of volume conservation, we have constructed a new asymptotic model capable of taking into account diffused pycnoclines and able to reconstruct analytically (apart from a standard one-dimensional numerical root finding when using smooth interpolating functions) the fluid velocity field associated with steady internal-wave propagation. The resulting model has the added benefit of providing an analytical starting point for a shear instability calculation, greatly simplifying most of the spectral computations of linearized stability.

Further refinements are also possible, though we leave them for future work. One such improvement could take place at the level of the reference two-layer model itself, following the recent model introduced by Makarenko & Maltseva (2008), by relaxing the homogeneous density assumption in the top layer with an exponential density profile. This would introduce an extra parameter in the optimal choice strategy, which could in principle allow for simultaneous matching of physical background fluid quantities, such as mass and potential energy. However, we remark that this new model refers only to stationary solutions, and to be useful for approximating solutions of the initial value problem of smoothly stratified Euler equations, it would be necessary to extend it to time-dependent problems. Improvements in the modelling of the intermediate layer could also be implemented. Thus, for instance, assessing the influence of an asymmetry in the vertical structure of the density stratification and velocity shear would be possible by a local modal decomposition in the pycnocline region. Similarly, interpolations other than linear could also be used, which would be relevant for the purpose of generating better balanced density-shear initial conditions for full Euler time-dependent simulations, thus preventing local shear instabilities in such simulations from growing to amplitudes known to be unphysical in certain situations. Fully time-dependent models governing the evolution of the pycnocline thickness probably constitute one of the most relevant extensions of the model we have introduced, and would allow for further testing the robustness of the proposed optimization strategy. The extension of the model to two horizontal dimensions is also possible and is perhaps the most interesting for geophysical applications. Finally, we remark that the current investigation could be easily adapted to configurations with multiple pycnoclines as well as to the case of a free (as opposed to rigid-lid) upper surface.

R.C. and R.T. gratefully acknowledge support from NSF through DMS-0509423, DMS CMG-0620687 and RTG DMS-0502266. The authors also acknowledge the help of David Adalsteinsson, who developed DataTank and was supported by NSF

https://doi.org/10.1017/S0022112010004891 Published online by Cambridge University Press

DMS-SCREMS 042241.651. Last but not least, we thank Wooyoung Choi for helpful discussions.

Appendix. Partial derivatives of optimizer functions $f_1 - f_4$

$$\frac{\partial f_1}{\partial z_0} = \overline{\rho}(z_0) - \rho_1, \tag{A 1}$$

$$\frac{\partial f_1}{\partial \rho_1} = H - z_0, \tag{A 2}$$

$$\frac{\partial f_2}{\partial z_0} = \frac{\left(z_0^3 - 2(H+h_0)z_0^2 + (H^2+5Hh_0+h_0^2)z_0 - 2Hh_0(H+h_0)\right) z_0\rho_1}{(H-z_0)^2(h_0-z)^2} - \overline{\rho}(z_0), \tag{A 3}$$

$$\frac{\partial f_2}{\partial \rho_1} = \frac{(H+h_0-z_0)z_0^2}{(H-z_0)(z_0-h_0)}, \tag{A 4}$$

$$\frac{\partial f_3}{\partial z_0} = z_0\left(\overline{\rho}(z_0) - \rho_1\right), \tag{A 5}$$

$$\frac{\partial f_3}{\partial \rho_1} = \frac{1}{2}\left(H^2 - z_0^2\right), \tag{A 6}$$

$$\frac{\partial f_4}{\partial z_0} = \frac{\left(2z_0^3 - 4(H+h_0)z_0^2 + 2(H^2+4Hh_0+h_0^2)z_0 - 3Hh_0(H+h_0)\right) z_0^2\rho_1}{2(H-z_0)^2(h_0-z)^2} - z_0\overline{\rho}(z_0), \tag{A 7}$$

$$\frac{\partial f_4}{\partial \rho_1} = \frac{(H+h_0-z_0)z_0^3}{2(H-z_0)(z_0-h_0)}, \tag{A 8}$$

where we have used

$$\frac{\partial r}{\partial z_0} = \overline{\rho}(z_0), \quad \frac{\partial W}{\partial z_0} = z_0\overline{\rho}(z_0). \tag{A 9}$$

REFERENCES

Camassa, R., Choi, W., Michallet, H., Rusås, P.-O. & Sveen, J. K. 2006 On the realm of validity of strongly nonlinear asymptotic approximations for internal waves. *J. Fluid Mech.* **549**, 1–23.

Camassa, R., Rusås, P.-O., Saxena, A. & Tiron, R. 2010 Fully nonlinear periodic internal waves in a two-fluid system of finite depth. *J. Fluid Mech.* **652**, 259–298.

Choi, W. & Camassa, R. 1999 Fully nonlinear internal waves in a two-fluid system. *J. Fluid Mech.* **396**, 1–36.

Fructus, D., Carr, M., Grue, J., Jensen, A. & Davies, P. 2009 Shear-induced breaking of large internal solitary waves. *J. Fluid Mech.* **620**, 1–29.

Fructus, D. & Grue, J. 2004 Fully nonlinear solitary waves in a layered stratified fluid. *J. Fluid Mech.* **505**, 323–347.

Grue, J., Jensen, A., Rusås, P.-O. & Sveen, J. K. 1999 Properties of large-amplitude internal waves. *J. Fluid Mech.* **380**, 257–278.

James, G. 2001 Internal traveling waves in the limit of a discontinuously stratified fluid. *Arch. Rat. Mech. Anal.* **160**, 41–90.

Lamb, H. 1932 *Hydrodynamics*, 6th edn. Cambridge University Press.

Lamb, K. G. & Wan, B. 1998 Conjugate flows and flat solitary waves for a continuously stratified fluid. *Phys. Fluids* **10**, 2061–2079.

https://doi.org/10.1017/S0022112010004891 Published online by Cambridge University Press

Love, A. E. H. 1891 Wave-motion in heterogeneous heavy fluids. *Proc. Lond. Math. Soc.* **22**, 307–316.

Makarenko, N. I. & Maltseva, J. L. 2008 An analytical model of large amplitude internal solitary waves. In *Extreme Ocean Waves* (ed. E. Pelinovsky & C. Kharif), pp. 179–189. Springer.

Miyata, M. 1985 An internal solitary wave of large amplitude. *La Mer* **23**, 4348.

Miyata, M. 1988 Long internal waves of large amplitude. In *Nonlinear Water Waves, IUTAM Symp., Tokyo 1987* (ed. K. Horikawa & H. Maruo), pp. 399–406. Springer.

Rusås, P.-O. 2001 On nonlinear internal waves in two- and three-layer fluids. DSc thesis, Department of Mathematics, University of Oslo.

Rusås, P.-O. & Grue, J. 2002 Solitary waves and conjugate flows in a three-layer fluid. *Eur. J. Mech.* B *Fluids* **21**, 185–206.

Sakai, T. & Redekopp, L. G. 2007 Models for strongly-nonlinear evolution of long internal waves in a two-layer stratification. *Nonlinear Process. Geophys.* **14**, 31–47.

Tiron, R. 2009 Strongly nonlinear internal waves in near two-layer stratifications: generation, propagation and self-induced shear instabilities. PhD thesis, Mathematics Department, University of North Carolina at Chapel Hill.

Tung, K. K., Chan, T. F. & Kubota, T. 1984 Large amplitude internal waves of permanent form. *Stud. Appl. Math.* **66**, 187–199.

Turkington, B., Eydeland, A. & Wang, S. 1991 A computational method for solitary internal waves in a continuously stratified fluid. *Stud. Appl. Math.* **85**, 93–127.

Yih, C.-S. 1969 Stratified flows. *Annu. Rev. Fluid Mech.* **1**, 73–110.

https://doi.org/10.1017/S0022112010004891 Published online by Cambridge University Press